Accepted Manuscript

Development of a hybrid FE-SEA-experimental model

A. Clot, J.W.R. Meggitt, R.S. Langley, A.S. Elliott, A.T. Moorhouse

Please cite this article as: A. Clot, J.W.R. Meggitt, R.S. Langley, A.S. Elliott, A.T. Moorhouse, Development of a hybrid FE-SEA-experimental model, *Journal of Sound and Vibration* (2019), doi: https://doi.org/10.1016/j.jsv.2019.03.027.

Development of a Hybrid FE-SEA-Experimental Model

A. Clot[1], J.W.R. Meggitt[2], R.S. Langley[1], A.S. Elliott[2], A.T. Moorhouse[2]

[1]*Department of Engineering, University of Cambridge*
[2]*Acoustics Research Centre, University of Salford*

Abstract

The vibro-acoustic response of complex structures with uncertain properties is a problem of great concern for modern industries. In recent years, much research has been devoted to the prediction of this response in the mid-frequency range where, because neither finite element analysis nor statistical energy analysis are appropriate, a hybrid deterministic-statistical approach becomes a suitable solution. Despite its potential, the existence of systems with active components that are too complex to be modelled numerically can limit the application of the method. However, it may still be possible to measure the dynamical response of these structures experimentally. This paper is hence concerned with the possibility of integrating experimental data into a hybrid deterministic-statistical method. To explain the new methodology, two similar case studies, consisting of a deterministic source structure that is coupled to a statistical plate receiver using passive isolators, are used. For each case, the vibratory excitation, characterised using in-situ blocked force measurements, the source structure mobility, and the isolators stiffness are experimentally determined and inserted in the proposed hybrid model of the system. The paper explains the techniques used for obtaining the considered experimental data and the theoretical model proposed for describing the systems. To validate the proposed approach, the predicted vibration response of the receiver plate is compared to the one obtained by experimentally randomising the plate in both case studies. The results show that a good agreement is obtained, both for the ensemble average response of the receiver structure and for the ensemble variance of this response. Moreover, the upper confidence bounds predicted by the hybrid method enclose well the ensemble of experimental results. The cause of some narrow-band differences observed between the predicted response and the experimental measurements is finally discussed. It is therefore concluded that the capabilities of the hybrid deterministic-statistical method can be clearly enhanced through the incorporation of experimental data prescribing active sub-systems.

Keywords: Statistical energy analysis; Experimental response; Hybrid modelling; Blocked forces

1. Introduction

The analysis of the vibro-acoustic response of complex structures becomes especially challenging as the wavelength of the propagating waves decreases with the increase of the frequency of excitation. In this

situation, the use of Finite Element (FE) models becomes unsuitable due to two main reasons: firstly, the number of degrees of freedom required to represent the system may be prohibitively large and secondly, the response becomes more and more sensitive to small imperfections that add uncertainty to the predicted response. Several alternatives that consider a smaller number of degrees of freedom than a FE formulation (being therefore more computationally efficient) have been presented in literature. Examples include the variational theory of complex rays [1] and the wave based method [2], both based on the the Trefftz approach. Another proposed approach is the use of efficient FE formulations, such as the discontinuous Galerkin method with plane waves and Lagrange multipliers [3]. At high-frequencies, both FE difficulties are successfully overcome by the Statistical Energy Analysis (SEA) approach, which allows prediction of the mean [4] and variance [4, 5] of an ensemble of nominally identical systems by solving a relatively simple power balance equation. Additional difficulties arise in the commonly termed 'mid-frequency range', the frequencies where neither FE analysis nor SEA are appropriate. Some authors have proposed methods that generalise the SEA formulation by, for example, employing a more detailed description of the system, as in the case of statistical modal energy distribution analysis (SmEdA) [6], or the vibrational conductivity approach [7]. A general wave-based approach for coupling both theories in a single model has been proposed by Shorter and Langley [8]. The approach, based on a diffuse field reciprocity result [9, 10], is briefly detailed in the next section. This hybrid FE-SEA approach has since been numerically and experimentally validated [11], demonstrating its use as a wide-band vibro-acoustic prediction tool. The method has been also extended with the development of expressions for determining the variance of the predicted response [12] and, more recently, with the inclusion of parametric uncertainties in the FE components of the system [13, 14]. Despite the capabilities and potential of the hybrid FE-SEA method, its applicability can be limited in those cases where the studied systems contain active structures that are too complex to be modelled numerically. In such cases, however, the dynamical response of these subsystems can still be measured experimentally, leading to the possibility of a combined experimental/numerical methodology.

The use of experimental data in SEA models has been considered by many researchers. Cimerman et al. [15] reviewed the use of test-based or Experimental SEA (ESEA) methods, in which the prediction rely on parameters experimentally determined. Bies and Hamid [16] proposed a power injection method to determine the internal and coupling loss factors of two coupled plates. The instabilities of their method were addressed by Lalor [17], who proposed an alternative ESEA formulation. Rosen and Borello [18] made ESEA available for industrial applications, by developing the SEA-XP software. The accuracy of the ESEA formulations has been also discussed by Hopkins [19], who tested methods to identify the wave conversion in T-junctions. More recently, Guasch [20] proposed an alternative method to determine coupling loss factors from energy transmissibility measurements. Despite its great interest, the experimental approach of ESEA methods differs from the one proposed here.

The independent characterisation of vibratory sources has been of interest to those within the field of

2

structural dynamics for many decades. Of the available quantities, there exist two fundamental descriptors of structural source activity. These are the blocked force and the free velocity [21]. In this work we are concerned primarily with the blocked force, and its application in the construction of a hybrid experimental/numerical model. The blocked force is defined as the force required to constrain the terminals of a vibration source such that their kinematics are constrained to zero. Direct measurement of the blocked force is complicated by the requirement of a sufficiently rigid termination which, in practice, can only be approximated over a limited frequency range. Recent work by Moorhouse et al. [22] has shown that the blocked force may instead be acquired in-situ (i.e. without removing the source from its intended installation) through an inverse procedure. The in-situ blocked force has since emerged as the most promising method towards the independent characterisation of structural sources and has found numerous applications within the automotive [23–31], aerospace [32], domestic product [33] and building acoustics [34] sectors. Whilst the in-situ blocked force approach has become well established, its experimental implementation is still an area of active research and its limitations must be acknowledged.

This paper is concerned in the use of experimental data to extend and enhance the applicability of the hybrid FE-SEA method. The paper presents two case studies where the excitation caused by a vibration source and the dynamic response of several mechanical components are experimentally characterised in a form that is suitable to be embedded in the hybrid method formulation. In Section 2, the general formulation of the hybrid FE-SEA-eXperimental method is presented. The formulation is used in Section 3 to develop a hybrid model for the case studies considered. Then, the responses predicted by the developed hybrid models are compared with experimental results in Section 4. Finally, the main conclusions of this work are summarised in Section 5.

2. Theoretical development

This section presents a brief outline of the theoretical background on which the development of a hybrid FE-SEA-X model is based. The key aspects of the hybrid FE-SEA method and the expressions used for predicting the mean and variance of the response of an ensemble of random systems are summarised in Section 2.1. The section ends with a description of the modifications applied to the hybrid equations in order to include systems with components that are experimentally characterised. Then, methodologies for characterising vibratory sources and vibration isolators are described in Sections 2.2 and 2.3, respectively.

2.1. The hybrid deterministic-statistical method

This section presents a brief outline of the general hybrid FE-SEA method formulation, with the addition of experimental terms. A detailed derivation of the presented expressions is given in [8] and [12].

2.1.1. Method overview and main assumptions

The hybrid FE-SEA formulation assumes that a built-up structure consists of a deterministic system which is coupled to a set of statistical subsystems. Each statistical subsystem is assumed to have random properties due to material or manufacturing imperfections. The deterministic system, modelled using the FE approach, is described by a set of degrees of freedom (DoF) representing the detailed deformation of the system; in contrast, each statistical subsystem is represented by only one DoF, its vibrational energy. The finite element model of the deterministic system yields a dynamic stiffness matrix $\mathbf{D}_\mathrm{d}$ which must be coupled to the statistical subsystems. This is done by representing the response of each subsystem as the sum of a "direct field" and a "reverberant field". The direct field is associated with waves generated at the connections to the FE model, and the coupling is accounted for through the addition of appropiate stiffness matrices to $\mathbf{D}_\mathrm{d}$. The reverberant (reflective) field is accounted for separately, as explained in Subsection 2.1.2.

As it will be detailed in the following subsections, the hybrid FE-SEA equations yield the mean and variance of the response of all the components of the built-up structure. The main assumptions of the method are:

- The response of each statistical subsystem (across its ensemble) constitutes a diffuse wavefield [9, 10].

- The subsystems are weakly coupled through the deterministic system. The hybrid method formulation considers the junctions between different statistical subsystems to be components of the deterministic system [8].

- The statistical subsystems are sufficiently random to ensure that the statistics of their isolated natural frequencies and mode shapes conform to the Gaussian Orthogonal Ensemble (GOE) [35].

2.1.2. Ensemble mean response

The first step in the application of the hybrid FE-SEA method is the identification of which parts of the vibro-acoustic system under consideration can be assumed to be deterministic and which ones are better described as statistical subsystems. The deterministic part is then represented by a finite set of degrees of freedom (DoF) $\mathbf{q}$ and the statistical part is defined by a set of subsystems, with each subsystem having a single degree of freedom (the vibrational energy E). As mentioned in the previous subsection, the wave field generated in each of the statistical subsystems can be understood as the combination of two fields: the response due to the initially generated waves (direct field), and the contribution from all the waves generated by the reflections at the subsystem's unknown boundaries (reverberant field). This separation can be used to define a direct field dynamic stiffness $\mathbf{D}_\mathrm{dir}$ for each subsystem. This matrix, which will be only populated for those DoF that define the deterministic boundaries of the subsystem, can be computed analytically for many simple cases or by a boundary element analysis in general. Then, the contribution of

4

the statistical subsystem k on $\mathbf{q}$ is taken into account by, first, adding $\mathbf{D}_{\text{dir}}^{(k)}$ to the dynamic stiffness of the deterministic part $\mathbf{D}_{\text{d}}$ and, second, including the forces arising from the existence of the reverberant field in each subsystem $\mathbf{f}_{\text{rev}}^{(k)}$. Then, for a given harmonic frequency ω, the governing equations of motion are [11]

$$\mathbf{D}_{\text{tot}}(\omega)\mathbf{q}(\omega) = \mathbf{f}_{\text{ext}}(\omega) + \sum_k \mathbf{f}_{\text{rev}}^{(k)}(\omega), \tag{1}$$

$$\mathbf{D}_{\text{tot}}(\omega) = \mathbf{D}_{\text{d}}(\omega) + \sum_k \mathbf{D}_{\text{dir}}^{(k)}(\omega), \tag{2}$$

where the ω dependence has been explicitly written for clarity, but will be later omitted for brevity, and where $\mathbf{D}_{\text{tot}}$ is the dynamic stiffness matrix of the deterministic part augmented by the direct field stiffness matrices of the considered subsystems. The force term $\mathbf{f}_{\text{ext}}$ is used to prescribe external forces to the deterministic part of the system, and that the reverberant force term $\mathbf{f}_{\text{rev}}^{(k)}$ describes, physically, the blocking force required to constrain the interface DoF of subsystem k in the presence of the reverberant field.

The key result to develop the hybrid FE-SEA method equations from Equations (1) and (2) is a reciprocity identity derived by Shorter and Langley [8] that relates the cross-spectral matrix of the reverberant forces of a subsystem k, denoted as $\mathbf{S}_{ff,\text{rev}}^{(k)}$, with its energy E_k and with its direct field dynamic stiffness matrix $\mathbf{D}_{\text{dir}}^{(k)}$. This relationship, valid when the ensemble response constitutes a diffuse random wavefield [10], can be expressed as

$$\mathbf{S}_{ff,\text{rev}}^{(k)} = \text{E}[\mathbf{f}_{\text{rev}}^{(k)}\mathbf{f}_{\text{rev}}^{(k)*T}] = \left(\frac{4E_k}{\pi\omega n_k}\right)\text{Im}\{\mathbf{D}_{\text{dir}}^{(k)}\}, \tag{3}$$

where $\text{E}[\ ]$ denotes the ensemble average and E_k and n_k are, respectively, the ensemble and time averaged vibrational energy and the ensemble averaged modal density of the subsystem.

An analysis of the energy flow in subsystem j leads to a power balance equation of the form [13]

$$\omega(\eta_j + \eta_{\text{d},j})E_j + \sum_k \omega\eta_{jk}n_j\left(\frac{E_j}{n_j} - \frac{E_k}{n_k}\right) = P_j + P_{\text{in},j}^{\text{ext}}, \tag{4}$$

where P_j and $P_{\text{in},j}^{\text{ext}}$ are the power inputs from external sources applied, respectively, on the subsystem and on the deterministic system, η_j is the loss factor of the subsystem, η_{jk} is a coupling loss factor and $\eta_{\text{d},j}$ is the loss factor term associated with the deterministic system. The detailed expressions for these items are [13]

$$\omega\eta_{\text{d},j} = \frac{2a_j}{\pi n_j}\sum_{r,s}\text{Im}\{D_{\text{d},rs}\}\left(\mathbf{D}_{\text{tot}}^{-1}\text{Im}\{\mathbf{D}_{\text{dir}}^{(j)}\}\mathbf{D}_{\text{tot}}^{-1*T}\right)_{rs}, \tag{5}$$

$$\omega\eta_{jk}n_j = \frac{2a_j}{\pi}\sum_{r,s}\text{Im}\{D_{\text{dir},rs}^{(j)}\}\left(\mathbf{D}_{\text{tot}}^{-1}\text{Im}\{\mathbf{D}_{\text{dir}}^{(k)}\}\mathbf{D}_{\text{tot}}^{-1*T}\right)_{rs}, \tag{6}$$

5

$$P_{\text{in},j}^{\text{ext}} = \frac{\omega}{2} \sum_{r,s} \text{Im}\{D_{\text{dir},rs}^{(j)}\} \left(\mathbf{D}_{\text{tot}}^{-1}\mathbf{S}_{ff}\mathbf{D}_{\text{tot}}^{-1*T}\right)_{rs}, \tag{7}$$

123 where the term a_j is included to take into account local concentrations in the wavefield [12, 36] and where
124 $\mathbf{S}_{ff}$ is the cross-spectral matrix of external forces. In Equations (5)-(7) the subscripts rs are used to identify
125 the rsth components of each matrix.

126 The hybrid FE-SEA method also yields the cross-spectral matrix of the response $\mathbf{q}$, which can be ex-
127 pressed as

$$\mathbf{S}_{qq} = \text{E}[\mathbf{q}\mathbf{q}^{*T}] = \mathbf{D}_{\text{tot}}^{-1} \left[\mathbf{S}_{ff} + \sum_k \left(\frac{4a_k E_k}{\pi \omega n_k}\right) \text{Im}\{\mathbf{D}_{\text{dir}}^{(k)}\}\right] \mathbf{D}_{\text{tot}}^{-1*T}. \tag{8}$$

128 The set of equations obtained by writing Equation (4) for each subsystem can be expressed in matrix
129 form:

$$\mathbf{C}_0\hat{\mathbf{E}} = \mathbf{P} + \mathbf{P}_{\text{in}}^{\text{ext}}, \tag{9}$$

130 where $\hat{E}_j = E_j/n_j$ is the ensemble averaged modal energy (i.e. the energy per mode) for subsystem j.
131 Equation (9), which has exactly the same form of the SEA equations [4], relates the power inputs applied
132 from external forces $\mathbf{P}$ and $\mathbf{P}_{\text{in}}^{\text{ext}}$ with the subsystem modal energies $\hat{\mathbf{E}}$. The entries of the matrix $\mathbf{C}_0$ can be
133 computed using Equations (5) and (6). Equation (9) can be solved to obtain the subsystem energies, and
134 these energies can then be substituted in Equation (8) to obtain the deterministic response.

135 *2.1.3. Ensemble variance response*

136 It is shown by Langley and Cotoni [12] that an expression in the form of Equation (9) can be written
137 for each member of the random ensemble as

$$\mathbf{C}\bar{\mathbf{E}} = \bar{\mathbf{P}} + \bar{\mathbf{P}}_{\text{in}}^{\text{ext}}, \tag{10}$$

138 where $\bar{E}_j$ is the modal energy of subsystem j (so that $\hat{\mathbf{E}} = E[\bar{\mathbf{E}}]$) and where the overbar on a quantity
139 indicates that it is referred to one member of the ensemble, instead of being an ensemble average. It follows
140 from a first order expansion in $\mathbf{C}$ [12] that $\mathbf{C}_0 = E[\mathbf{C}]$. Therefore, $\bar{\mathbf{P}}$, $\bar{\mathbf{P}}_{\text{in}}^{\text{ext}}$ and $\mathbf{C}$ vary randomly across the
141 ensemble but, their mean values can be computed from Equations (4)-(7).

142 Then, the ensemble covariance of the subsystem modal energies $\bar{E}_i$ and $\bar{E}_j$ is obtained by considering a
143 first order perturbation expansion of Equation (10). It has been shown in [12] that this covariance can be
144 expressed as

6

$$\text{Cov}\left[\bar{E}_i, \bar{E}_j\right] = \sum_k \sum_s C_{0,ik}^{-1} C_{0,js}^{-1} \text{Cov}[\bar{P}_k + \bar{P}_{\text{in},k}^{\text{ext}}, \bar{P}_s + \bar{P}_{\text{in},s}^{\text{ext}}]$$

$$+ \sum_k \sum_s \sum_{r \neq k} [(C_{0,ik}^{-1} - C_{0,ir}^{-1})C_{0,js}^{-1} + (C_{0,jk}^{-1} - C_{0,jr}^{-1})C_{0,is}^{-1}] \hat{E}_r \text{Cov}[C_{kr}, \bar{P}_s + \bar{P}_{\text{in},s}^{\text{ext}}] \tag{11}$$

$$+ \sum_k \sum_p \sum_{s \neq k} \sum_{r \neq p} (C_{0,ik}^{-1} - C_{0,is}^{-1})(C_{0,jp}^{-1} - C_{0,jr}^{-1}) \hat{E}_s \hat{E}_r \text{Cov}[C_{ks}, C_{pr}],$$

where the $C_{0,jk}^{-1}$ represents the jkth component of $\mathbf{C}_0^{-1}$. The covariance terms on the right-hand side of Equation (11) can be derived by using random matrix theory and Equation (3). A detailed derivation of these terms can be found in [12] and, for the sake of brevity, general expressions for these terms will not be repeated here. However, the particular expressions used for the case studies considered in this work will be presented in Subsection 3.6. It is important to mention that, once the hybrid mean equations have been solved, all the right-hand side terms of Equation (11) are known quantities.

The randomness in the subsystems leads to randomness in the response of the deterministic system. Langley and Cotoni [12] have shown that the ensemble variance of $\mathbf{S}_{qq}$ is given by

$$\text{Var}[(\mathbf{S}_{qq})_{ij}] = 2(\mathbf{D}_{\text{tot}}^{-1} \mathbf{S}_{ff} \mathbf{D}_{\text{tot}}^{-1*T})_{ij} \sum_k \hat{E}_k G_{ij}^{(k)}$$

$$+ \sum_{k,s} \{2\text{Cov}[\bar{E}_k, \bar{E}_s] + \hat{E}_k \hat{E}_s\} G_{ij}^{(k)} G_{ij}^{(s)}, \tag{12}$$

where

$$\mathbf{G}^{(k)} = \left(\frac{4a_k}{\omega\pi}\right) \mathbf{D}_{\text{tot}}^{-1} \text{Im}\{\mathbf{D}_{\text{dir}}^{(k)}\} \mathbf{D}_{\text{tot}}^{-1*T}. \tag{13}$$

As in the case of the ensemble average response, once Equation (11) has been solved to obtain the subsystem covariances $\text{Cov}\left[\bar{E}_i, \bar{E}_j\right]$, these can be substituted in Equation (12) to determine the deterministic system variance $\text{Var}[(\mathbf{S}_{qq})_{ij}]$.

2.1.4. Hybrid FE-SEA-X method

The hybrid FE-SEA method can be enhanced by considering that some of the deterministic components of the system are modelled using experimental data instead of using a FE or an analytical approach. This experimental data can be characterising either a passive quantity or an active quantity of the structure. More precisely, the dynamic stiffness matrix of the deterministic part of the system, $\mathbf{D}_{\text{d}}$, can be assumed to be composed as a combination of a numerically/analytically determined dynamic stiffness matrix $\mathbf{D}_{\text{d,FE}}$ and one or more experimentally determined dynamic stiffness matrices $\mathbf{D}_{\text{d,exp}}^{(j)}$. Then

$$\mathbf{D}_{\text{d}} = \mathbf{D}_{\text{d,FE}} + \sum_j \mathbf{D}_{\text{d,exp}}^{(j)}, \tag{14}$$

7

where, the summation represents the assembly of the various matrices in the conventional fashion.

A similar decomposition can be considered for the cross-spectral matrix of external forces, which can be expressed as

$$\mathbf{S}_{ff} = \mathbf{S}_{ff,\text{FE}} + \sum_j \mathbf{S}_{ff,\text{exp}}^{(j)}, \tag{15}$$

where $\mathbf{S}_{ff,\text{exp}}^{(j)}$ is an experimentally determined cross-spectral blocked force matrix.

The procedures necessary for experimentally determining $\mathbf{D}_{\text{d,exp}}^{(j)}$ and $\mathbf{S}_{ff,\text{exp}}^{(j)}$ will be discussed in the following.

2.2. Characterisation of structure-borne sound sources

A vibratory source is an active sub-system that generates a disturbance as a result of some internal, often inaccessible, mechanism. Unlike passive sub-systems, a vibratory source is characterised by two parameters. The first, a passive quantity describing the source's ability to transfer energy, and the second, an active quantity describing the operational behaviour of the source. In the context of the hybrid FE-SEA-X method discussed above, these quantities are characterised, *independently*, by the sub-system's free interface dynamic stiffness matrix, $\mathbf{D}_{\text{d,exp}}$, and blocked force, $\bar{\mathbf{f}}$, respectively.

2.2.1. Free interface dynamic stiffness matrix

The free interface dynamic stiffness matrix, $\mathbf{D}_{\text{d,exp}}^{(S)}$, of an experimental sub-system S describes the force on each DoF when another DoF is displaced, whilst all others are fixed. This constraint makes the direct measurement of $\mathbf{D}_{\text{d,exp}}^{(S)}$ impractical. Instead, it may be determined through its inverse relationship with some measurable frequency response function (FRF) matrix, for example, the free mobility.

The free mobility of a sub-system with M interface DoF, $\mathbf{Y}_S \in \mathbb{C}^{M \times M}$, is an independent characterisation of its passive properties and is defined by the velocity/force ratios at and between its interface DoF whilst uncoupled and freely suspended. Analogous quantities include the free acceleration and the free receptance, which are related to the free mobility through integration and differentiation, respectively.

Experimentally, a close approximation to the free mobility is achieved by resiliently suspending the sub-system and measuring its interface dynamics directly. However, if the sub-system is very large, or too lightweight, resilient suspension may not be practical or yield a suitable free boundary condition. In this case decoupling procedures may be required [37, 38]. Alternatively, the source mobility may be obtained, in theory, from a numerical model.

Once acquired, the free mobility may be used to determine the free interface dynamic stiffness matrix required by the hybrid method,

$$\mathbf{D}_{\text{d,exp}}^{(S)} = \mathrm{i}\omega \mathbf{Y}_S^{-1}. \tag{16}$$

8

193 It is important to note that the inversion of measured FRF matrices is an important source of errors in

194 experimental sub-structuring [39]. Care should therefore be taken to ensure that a reliable $\mathbf{Y}_S$ is obtained.

2.2.2. In-situ blocked force

196 The blocked force is a fundamental descriptor of structural source activity and is defined as the force

197 required to block the terminals of a vibration source such that their velocity is zero (see Figure 1a) [21]. It

198 was shown by Moorhouse et al. [22] that the blocked force may be determined 'in-situ' through an inverse

199 procedure. The relation of note is given by,

$$\mathbf{v}_{C_b} = \mathbf{Y}_{C_{bc}} \bar{\mathbf{f}}_{S_c}, \tag{17}$$

200 where $\mathbf{Y}_{C_{bc}} \in \mathbb{C}^{N \times M}$ is the measured mobility matrix of the coupled assembly in which the source is

201 installed, $\mathbf{v}_{C_b} \in \mathbb{C}^N$ is a measured operational velocity vector, and $\bar{\mathbf{f}}_{S_c} \in \mathbb{C}^M$ is the vector of unknown

202 blocked forces. Here, subscripts b and c represent remote receiver and coupling interface DoFs, respectively.

203 For $N = M$, providing that the measured mobility matrix is of full rank, a unique solution is found through

204 the inverse mobility matrix $\mathbf{Y}_{C_{bc}}^{-1}$. For $N > M$, the Moore-Penrose pseudo inverse [40] may be used in place

205 of the classical matrix inverse, leading to a least squares solution of the problem. The remote DoFs b are

206 collocated with the DoFs c when measurements are performed solely at the coupling interface. In such a case

207 over-determination may be achieved by including an additional set of remote DoFs, such that the interface

208 DoFs are a subset of those used to determine the blocked forces.

209 The experimental implementation of Equation (17) requires a two part measurement procedure. In part

210 one, the source is turned on and the operational velocity, $\mathbf{v}_{C_b}$, is measured. In the other, the source is turned

211 off and the mobility matrix, $\mathbf{Y}_{C_{bc}}$, is measured.

212 Once the blocked forces related to a vibratory source are determined, they can be used to compute the

213 associated experimental cross-spectral blocked force matrix as follows

$$\mathbf{S}_{ff,\mathrm{exp}}^{(j)} = \bar{\mathbf{f}}_{S_c} \bar{\mathbf{f}}_{S_c}^{*T}. \tag{18}$$

214 This cross-spectral matrix can then be used to compute the cross-spectral matrix of external forces $\mathbf{S}_{ff}$
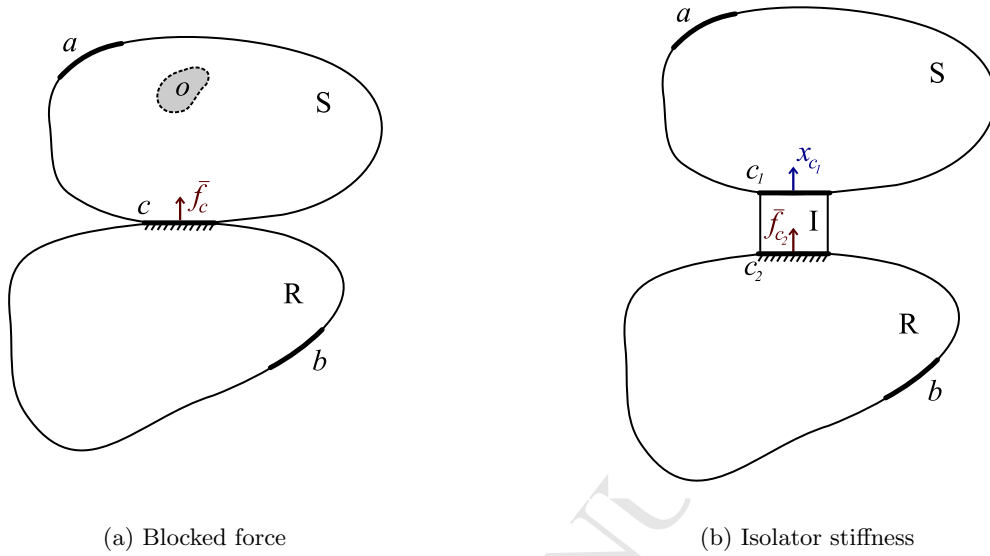
215 using Equation (15).

9

(a) Blocked force   (b) Isolator stiffness

Figure 1: Diagrams for blocked force and isolator characterization.

2.3. Characterisation of vibration isolators

It is typical to place vibratory sources on resilient foundations or footings so as to reduce the severity of their transmitted vibration. It is important therefore to be able to correctly characterise the properties of such elements in a way that they may be included in a hybrid model.

The preferred quantity for the characterisation of a resilient element is the dynamic transfer stiffness [41], defined as the ratio of the applied displacement at one interface to the blocked force at the other (see Figure 1b). The dynamic transfer stiffness is an independent property of the element and therefore invariant to changes in the dynamics of source and receiver sub-systems (neglecting compressional effects such as pre-load). Whilst there exist standardised methods for the determination of dynamic transfer stiffness [42], they require elements to be removed from their intended installation and installed within specialized test rigs. This is not only inconvenient but arguably places the coupling element under a non-representative mounting condition. An alternative procedure was recently proposed by Meggitt et al. [43], where a coupling interface mobility matrix $\mathbf{Y}_C$ is measured and subsequently inverted, yielding a pair of independent transfer impedances, $\mathbf{Z}_{I_{c1c2}}$ and $\mathbf{Z}_{I_{c2c1}}$,

$$\begin{bmatrix} \mathbf{Z}_{C_{c1c1}} & \mathbf{Z}_{I_{c1c2}} \\ \mathbf{Z}_{I_{c2c1}} & \mathbf{Z}_{C_{c2c2}} \end{bmatrix} = \begin{bmatrix} \mathbf{Y}_{C_{c1c1}} & \mathbf{Y}_{C_{c1c2}} \\ \mathbf{Y}_{C_{c2c1}} & \mathbf{Y}_{C_{c2c2}} \end{bmatrix}^{-1}. \tag{19}$$

Once acquired, the transfer impedance may be related to the dynamic transfer stiffness through,

$$\mathbf{K}_{I_{c1c2}} = \mathrm{i}\omega\mathbf{Z}_{I_{c1c2}}. \tag{20}$$

231 This approach has been validated and shown to provide an independent and broad-band characterisation

232 suitable for the hybrid method [43, 44]. Note that the in-situ method discussed above is related to a more

233 general class of characterisation techniques referred to as inverse sub-structuring.

234 Having determined the dynamic transfer stiffness of the element, an appropriate stiffness matrix $\mathbf{D}_{\mathrm{d,exp}}^{(I)}$

235 must be formulated for use within the hybrid model. Assuming simple spring like behavior $\mathbf{D}_{\mathrm{d,exp}}^{(I)}$ may be

236 approximated as,

$$\mathbf{D}_{\mathrm{d,exp}}^{(I)} = \left[\begin{array}{cc} -\mathbf{K}_{I_{c1c2}} & \mathbf{K}_{I_{c1c2}} \\ \mathbf{K}_{I_{c1c2}} & -\mathbf{K}_{I_{c1c2}} \end{array} \right]. \tag{21}$$

237 The above construction is only valid whilst force is conserved across the element, i.e. below its first internal

238 resonance. If the coupling element possesses significant internal dynamics and/or requires rotational DoFs

239 an alternative construction of $\mathbf{D}_{\mathrm{d,exp}}^{(I)}$ may be required.

240 3. Hybrid model for a case study

241 As a means of illustrating the construction of a hybrid model, two case study structures are considered

242 in this paper. Both structures consist of a vibration source coupled resiliently to a large thin plate. In

243 this section, a brief description of these case studies is followed by the definition of the deterministic and

244 random parts of the hybrid model developed to represent them. Then, expressions for the matrices $\mathbf{D}_{\mathrm{d}}$, $\mathbf{S}_{ff}$

245 and $\mathbf{D}_{\mathrm{dir}}$ are detailed and, finally, the energy mean and energy variance expressions required for these case

246 studies are presented.

247 3.1. Description of the case studies considered

248 Figures 2a and 2b show the two case studies considered in this work. In both cases the vibration source is

249 connected to a large thin receiver plate using four resilient elements. In the first study, the source subsystem

250 is an electric pump that does not allow a direct access to the coupling interface, adding difficulties to its

251 experimental characterisation. In the second, the source consists of a servomotor bolted to a small aluminium

252 plate, and this small plate is bolted to four steel feet which have been designed to facilitate the placement

253 of sensors in the coupling interface between the vibration source and the resilient elements. In each case

254 study, resilient elements of an appropriate size are used. Figure 2b also shows the positions of the set of

255 accelerometers used to measure the response and some of the additional small masses used to randomise

256 the large thin plate to produce an ensemble of systems. Additional information regarding the experimental

257 setup can be found in Section 4.

258 The hybrid model of the case studies is developed by determining, for each of them, the matrices $\mathbf{D}_{\mathrm{d}}$

259 and $\mathbf{S}_{ff}$ experimentally. Therefore, the model does not contain any FE component and only the second

260 right-hand side term in Equations (14) and (15) is considered.

11
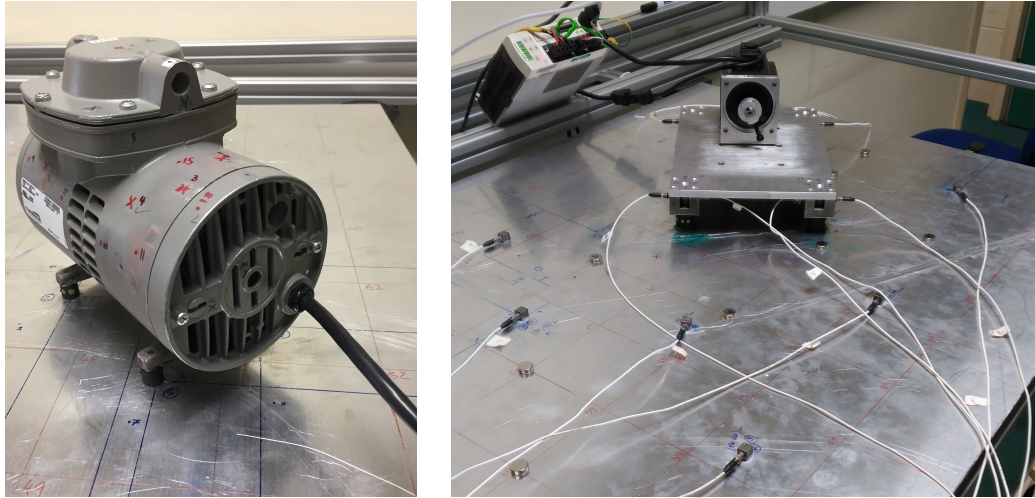
(a) Source-isolators-plate setup for the first case study

(b) Experimental setup for the second case study, with the added masses and the measuring accelerometers on the large thin plate.

Figure 2: Case studies considered

3.2. Definition of the deterministic and statistical parts of the case studies

The case studies are modelled using the hybrid method by considering the vibration source and the four isolators to compose the deterministic part of the structure, and the large receiver plate, to be the (only) statistical subsystem. In order to compute the ensemble mean response of the statistical subsystem it is necessary to derive expressions for the matrices that appear in Equations (5) and (7) (Equation (6) is not computed in a hybrid model that has only one statistical subsystem). The size of these matrices depends on how many DoFs are considered for the deterministic part of the hybrid model.

The aim of the present work is to characterise the dynamical properties of the deterministic subsystem (as represented by $\mathbf{D}_\mathrm{d}$), using experimentally determined properties. Therefore, the response at the DoF considered should be easily (directly or indirectly) measured. It has been assumed that, due to the type of coupling that exists between the different components of the system, it is sufficient to consider the vertical response at points situated at the top and base of the four isolator feet in order to model the system. Then, DoF q_1 to q_4 are defined at the contact between the source system and the top of the isolators, and DoF q_5 to q_8 are defined at the contact between the bottom of the isolators and the large receiver thin plate. A scheme with the position and number of each one of these eight DoF for the second case study is presented in Figure 3. The same positions and numbering are considered for the first case study.
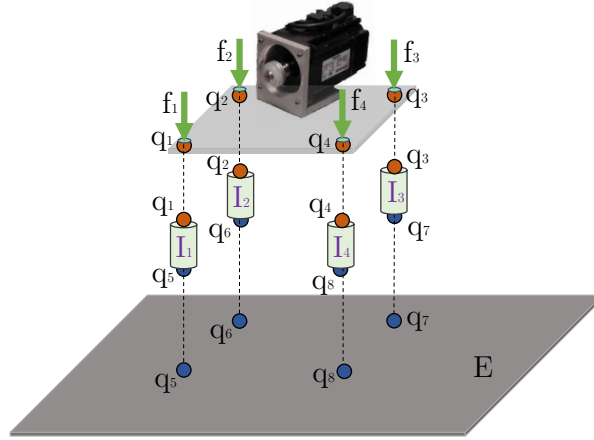
Figure 3: Scheme of the hybrid model used in both case studies, with the considered degrees of freedom and the external forces depicted.

3.3. Determination of $\boldsymbol{D}_d$ from experimental measurements

The dynamic stiffness matrix of the deterministic part of the system can be expressed as a combination of the experimental dynamic stiffness matrices of the vibration source $\mathbf{D}_{d,\exp}^{(S)}$ and of the experimental dynamic stiffness matrices of each one of the four isolators $\mathbf{D}_{d,\exp}^{(I_k)}$ $(k = 1, \ldots, 4)$. With the DoF considered $\mathbf{D}_{d,\exp}^{(S)}$ is a 4×4 matrix obtained from Equation (16), and each $\mathbf{D}_{d,\exp}^{(I_k)}$ is a 2×2 matrix obtained from Equation (21). The experimental and numerical procedures performed to obtain both matrices have been described in Sections 2.2.1 and 2.3.

Once the frequency response functions of the deterministic components have been experimentally determined, they are combined to obtain the experimental $\mathbf{D}_d$. This matrix can be written as

$$
\mathbf{D}_d = \begin{bmatrix}
d_{11}^{(S)}+d_{11}^{(I_1)} & d_{12}^{(S)} & d_{13}^{(S)} & d_{14}^{(S)} & d_{15}^{(I_1)} & 0 & 0 & 0 \\
d_{21}^{(S)} & d_{22}^{(S)}+d_{22}^{(I_2)} & d_{23}^{(S)} & d_{24}^{(S)} & 0 & d_{26}^{(I_2)} & 0 & 0 \\
d_{31}^{(S)} & d_{32}^{(S)} & d_{33}^{(S)}+d_{33}^{(I_3)} & d_{34}^{(S)} & 0 & 0 & d_{37}^{(I_3)} & 0 \\
d_{41}^{(S)} & d_{42}^{(S)} & d_{43}^{(S)} & d_{44}^{(S)}+d_{44}^{(I_4)} & 0 & 0 & 0 & d_{48}^{(I_4)} \\
d_{51}^{(I_1)} & 0 & 0 & 0 & d_{55}^{(I_1)} & 0 & 0 & 0 \\
0 & d_{62}^{(I_2)} & 0 & 0 & 0 & d_{66}^{(I_2)} & 0 & 0 \\
0 & 0 & d_{73}^{(I_3)} & 0 & 0 & 0 & d_{77}^{(I_3)} & 0 \\
0 & 0 & 0 & d_{84}^{(I_4)} & 0 & 0 & 0 & d_{88}^{(I_4)}
\end{bmatrix},
\tag{22}
$$

where $d_{ij}^{(S)}$ represents the ijth component of $\mathbf{D}_S$, and $d_{ij}^{(I_k)}$ represents the ijth component of $\mathbf{D}_{I_k}$.

3.4. Determination of $\boldsymbol{S}_{ff}$ from experimental measurements

The cross-spectral matrix of external forces $\mathbf{S}_{ff} = \mathbf{ff}^{*T}$ is computed using the set of forces acting on the eight DoF considered. In order to do that, the blocked forces that characterise the operational behaviour of the vibration source are experimentally obtained using the in-situ procedure described in Section 2.2.2. This characterisation, which requires measurement at the coupling interface between the source and receiver

13

292 parts of the structure, has been performed considering that this coupling interface is defined by the DoF q_1
293 to q_4. Therefore, the force vector acting on both case studies is

$$\mathbf{f} = \begin{pmatrix} \bar{f}_1 & \bar{f}_2 & \bar{f}_3 & \bar{f}_4 & 0 & 0 & 0 & 0 \end{pmatrix}^T, \tag{23}$$

294 where, for each case study and for each type of excitation considered, the blocked forces $\bar{f}_i$ are determined
295 using Equation (17).

296 *3.5. Determination of $\boldsymbol{D}_{dir}$ for the case studies*

297 The direct field dynamic stiffness matrix for a set of point contacts on a statistical thin plate can be
298 computed using analytical techniques. As the deterministic boundaries for the case study considered are
299 simply the DoF q_5 to q_8, $\mathbf{D}_{\mathrm{dir}}$ can be easily computed using the analytical expression of the transverse
300 response of an infinite thin plate to a vertical point load (due to the type of coupling that exists between
301 the plate and the isolators, it has been assumed that the effect of the in-plane forces and bending moments
302 can be neglected). The response at a position i due to a point load applied at a position j can be expressed
303 as [45]

$$H_{ij} = H(r_{ij}) = \frac{H_0^{(2)}(k_B r_{ij}) - 2\mathrm{i}/\pi K_0(k_B r_{ij})}{8\mathrm{i}\omega\sqrt{D\rho h}}, \tag{24}$$

304 where r_{ij} is the distance between both positions, $H_0^{(2)}$ is the Hankel function of the second kind and zeroth
305 order, K_0 is the modified Bessel function of the second kind and zeroth order, D is the flexural rigidity of
306 the plate, ρ is its mass density, h is its thickness and $k_B = \left(\rho h \omega^2 / D\right)^{1/4}$ is the plate bending wavenumber.
307 Equation (24) can be used to build a 4×4 matrix of plate receptances $\mathbf{H}$ that defines the response at
308 the boundary DoF q_5 to q_8. The matrix $\mathbf{D}_{\mathrm{dir}}$ can then be simply obtained by inverting $\mathbf{H}$ and inflating the
309 resulting matrix to the eight DoF considered. This yields

$$\mathbf{D}_{\mathrm{dir}} = \begin{bmatrix} \mathbf{0}_{4\times4} & \mathbf{0}_{4\times4} \\ \mathbf{0}_{4\times4} & \mathbf{H}^{-1} \end{bmatrix}, \tag{25}$$

310 where $\mathbf{0}_{4\times4}$ denotes a 4×4 matrix of zeros.

311 *3.6. Energy mean and variance expressions for the case studies*

312 In both case studies the structure is modelled considering only one statistical subsystem, and external
313 forces are only applied on the deterministic part of the system. Therefore, Equation (4) reduces to

$$\omega(\eta + \eta_{\mathrm{d}})E = P_{\mathrm{in}}^{\mathrm{ext}}, \tag{26}$$

14

314 where the subsystem subscripts have been omitted, and where $\omega\eta_{\mathrm{d}}$ and $P_{\mathrm{in}}^{\mathrm{ext}}$ are computed using Equations

315 (5) and (7). Furthermore, the covariance expression defined by Equation (11) is reduced to the variance of

316 the subsystem modal energy, which can be written as

$$\mathrm{Var}[\bar{E}] = C_0^{-2}\mathrm{Var}[\bar{P}_{\mathrm{in}}^{\mathrm{ext}}] = C_0^{-2}\mathrm{Relvar}[\bar{P}_{\mathrm{in}}^{\mathrm{ext}}]\mathrm{E}[\bar{P}_{\mathrm{in}}^{\mathrm{ext}}]^2. \tag{27}$$

317 In this case, the matrix $\mathbf{C}_0$ defined in Equation (9) is reduced to $C_0 = \omega(\eta + \eta_{\mathrm{d}})n$, and the value of

318 $\mathrm{E}[\bar{P}_{\mathrm{in}}^{\mathrm{ext}}]$ can be again computed using Equation (7). The relative variance of the power input $\mathrm{Relvar}[\bar{P}_{\mathrm{in}}^{\mathrm{ext}}]$

319 is computed using the general expression for the relative covariance of the power inputs applied to different

320 subsystems presented in [12]. For a system composed of only one statistical subsystem, this expression is

321 reduced to

$$\mathrm{Relvar}[\bar{P}_{\mathrm{in}}^{\mathrm{ext}}] = \frac{a}{\pi m'}\left[\frac{\mathbf{q}^{(0),*T}\mathbf{J}\mathbf{q}^{(0)}}{\mathbf{q}^{(0),*T}\mathrm{Im}\{\mathbf{D}_{\mathrm{dir}}\}\mathbf{q}^{(0)}}\right]. \tag{28}$$

322 In Equation (28), $\mathbf{q}^{(0)} = \mathbf{D}_{\mathrm{tot}}^{-1}\mathbf{f}$ is the zeroth order term in the perturbation expansion used in [12] to

323 obtain an approximate solution of the equation of motion of the master system. In the considered case

324 studies, the vector of external forces $\mathbf{f}$ is the vector of blocked forces defined in Equation (23). Additionally,

325 $m' = \omega\eta'n$ is the effective modal overlap of the subsystem, with $\eta' = 1/(\omega n C_0^{-1})$ being the effective in-situ

326 loss factor [4]. As before, the parameter a takes into account local concentrations in the wavefield [12, 36].

327 Finally, for a single subsystem the Hermitian matrix $\mathbf{J}$ takes the following form

$$\begin{aligned}\mathbf{J} =&\, 4\mathrm{Im}\{\mathbf{D}_{\mathrm{dir}}\}\mathbf{D}_{\mathrm{tot}}^{-1}\mathrm{Im}\{\mathbf{D}_{\mathrm{dir}}\}\mathbf{D}_{\mathrm{tot}}^{-1*T}\mathrm{Im}\{\mathbf{D}_{\mathrm{dir}}\} + \mathrm{Im}\{\mathbf{D}_{\mathrm{dir}}\}\\ &- 2i\mathrm{Im}\{\mathbf{D}_{\mathrm{dir}}\}\mathbf{D}_{\mathrm{tot}}^{-1}\mathrm{Im}\{\mathbf{D}_{\mathrm{dir}}\} + 2i\mathrm{Im}\{\mathbf{D}_{\mathrm{dir}}\}\mathbf{D}_{\mathrm{tot}}^{-1*T}\mathrm{Im}\{\mathbf{D}_{\mathrm{dir}}\}.\end{aligned} \tag{29}$$

328 4. Comparison with experimental results

329 4.1. Case study I: electric pump/isolators/damped plate

330 4.1.1. The test system and the experimental setup

331 The first case study considered in this work, shown in Figure 2a, consisted of an electric pump connected

332 to a receiver large thin plate using four resilient elements. This type of vibration source is a realistic source

333 likely encountered in practice. The construction of a hybrid model for this assembly required to characterise

334 experimentally the source mobility, the blocked forces acting on the source-isolators interface (for each type

335 of excitation considered) and the dynamic stiffness of the isolators.

336 For the measurement of its free mobility $\mathbf{Y}_S$, the source was suspended on soft elastic bungees. Each

337 foot was instrumented with a single accelerometer, located directly above the coupling interface. Due to

restricted interface access, excitations were applied from beneath. A spaced pair of excitations were applied at each interface DoF. Appropriate averaging and sign corrections returned the free source mobility.

In the characterisation of its blocked force the source was resiliently coupled to a second assembly. With access to the coupling interface restricted the blocked force was determined using remote receiver DoFs b only. A two fold over-determination was achieved using eight remote DoFs. The transfer mobility between the coupling interface and each remote DoF b_i was measured reciprocally. The operational velocities at b were measured for both operational and artificial excitation conditions. For repeatability the operational velocities due to the artificial excitation were normalised to the input force. The blocked forces were subsequently calculated as per Section 2.2.2.

The four resilient elements used in this case study (type: Fibet 1413vv10-60) were assumed to have nominally identical stiffness values. As such only a single element was characterised. This was done using the in-situ approach presented in Section 2.3. The resilient element was placed in a mass-isolator-mass assembly, as illustrated in Figure 1b, for characterization prior to constructing the main assembly. A spaced pair of accelerometers were mounted above and below the coupling element and excitations performed at each. The resulting mobilities were averaged appropriately to yield the coupling interface mobility matrix, $\mathbf{Y}_C \in \mathbb{C}^{2\times2}$. The element's transfer stiffness was then determined as per Equations (19) and (20). The resilient elements were characterised only in the vertical translational DoFs, i.e. in-plane and rotational components were neglected. This was justified based on previous success when using the same source and coupling elements in an experimental sub-structuring prediction [46]. Similarly, for the resilient elements used in case study two experimental evidence in [47] justified this approximation. Furthermore, inspection of the transfer stiffness obtained (for both case studies) revealed that there were no significant dynamics (i.e. internal mount resonances) in the frequency range considered, thus enabling the use of Equation (21) to approximate the element stiffness matrix.

The receiver subsystem was a large aluminium rectangular thin plate of dimensions $L_1 = 1$ m, $L_2 = 0.8$ m and thickness $h = 3$ mm. The mechanical parameters considered for the aluminium were density $\rho = 2700$ kg·m^{-3}, Young modulus $E = 70$ GPa, and Poisson ratio $\nu = 0.33$. The modal density was computed using the asymptotic expression for the bending modes of a thin plate [4] $n = L_1 L_2 / 4\pi\sqrt{\rho h / D}$, giving $n = 0.013$ modes/(rad/s). The edges of the plate were supported on an external structure and the damping of the structure was increased by gluing viscoelastic damping patches to the plate structure. The loss factor of the plate was experimentally determined from its response without the deterministic subsystem, i.e. the source and the four isolators, placed on it. The loss factor was slightly frequency dependent, with an average value of $\eta = 2.3\%$ in the frequency range studied (1-1250 Hz). With these values, the modal overlap factor of the plate at 1000 Hz is $m = \omega n \eta = 1.87$.

In order to create an ensemble of subsystems, the plate response was randomised experimentally by adding seven small masses at randomly chosen locations. The total mass added was 650 g, approximately

16

373 10% of the initial mass of the plate.

374   As a first step in the performed comparisons, the experimental response of the receiver plate was studied

375 prior to attach the electric pump and the isolators on it. After that, two types of excitations were studied

376 with the source subsystem coupled to the receiver plate: an impact excitation applied on the source structure

377 using an instrumented hammer and the excitation caused by the electric pump operating at constant speed.

378 A summary of the results presented for this case study (and for the one described in Section 4.2) can be

379 found in Table 1.

Figure	Case study	Response type	Excitation
4	Case 1:Bare plate	Plate E	Impact
5	Case 1:Pump/isolator/plate	Plate $|v|^2$	Impact
6,7	Case 1:Pump/isolator/plate	Plate $|v|^2$	Operational
8	Case 2:Motor/isolator/plate	Plate $|v|^2$	Impact
9	Case 2:Motor/isolator/plate	Plate E	Impact
10	Case 2:Motor/isolator/plate	Plate $|v|^2$	Operational
11	Case 2:Motor/isolator/plate	Plate E	Operational

Table 1: Summary of the results presented in Section 4.

380 *4.1.2. Receiver plate ensemble average and variance comparison*

381   To study the experimental response of the receiver plate, an impact excitation was applied on it using

382 an instrumented hammer and, in order to have a space average of the plate vibration, the response was

383 measured at four different positions. The responses per unit force were computed dividing the measured

384 acceleration spectra by the measured force spectrum. The response of an ensemble of subsystems was

385 obtained by performing the test 20 times with different mass locations each time.

386   The vibration energy of the plate has been estimated from the experimental results by averaging the

387 response of each test over the four accelerometers to give $\langle |v|^2 \rangle_\text{a}$, and then noting that $E = m_\text{p} \langle |v|^2 \rangle_\text{a}/2$.

388 With this approach, an ensemble of 20 experimental estimations of the plate energy has been obtained.

389   The response of the plate has been predicted by considering a hybrid FE-SEA model of the system. The

390 model consists of a trivial deterministic system with a single DoF, the position where the hammer impacts

391 were applied, and one statistical subsystem, the whole plate. The predicted response per unit force has

392 been obtained by considering a vertical unitary force at the only DoF of the system. The matrices that

393 appear in Equations (5) and (7) are then scalars with the following expressions: $D_\text{d} = 0$, $S_{ff} = 1$ and

394 $D_\text{dir} = 8\mathrm{i}\omega\sqrt{D\rho h}$.

17

A comparison between the experimental vibrational energy of the plate and the energy predicted by the hybrid model, computed using Equation (26), is shown in Figure 4(a). The experimental relative variance of the energy, i.e. the variance divided by the square of the expected value, has been compared with the predicted relative variance, computed using Equations (26) and (27), in Figure 4(b). This predicted relative variance has been used to obtain the upper Confidence Interval (CI) for a 95% Confidence Level (CL), and for a 99% CL shown in the energy comparison. These upper bounds have been computed using the procedure detailed in Appendix C of [48], which assumes that the statistical distribution of the plate energy is lognormal. The use of a lognormal probability density function for the energy of a random system has been theoretically justified by Langley et al. [49].
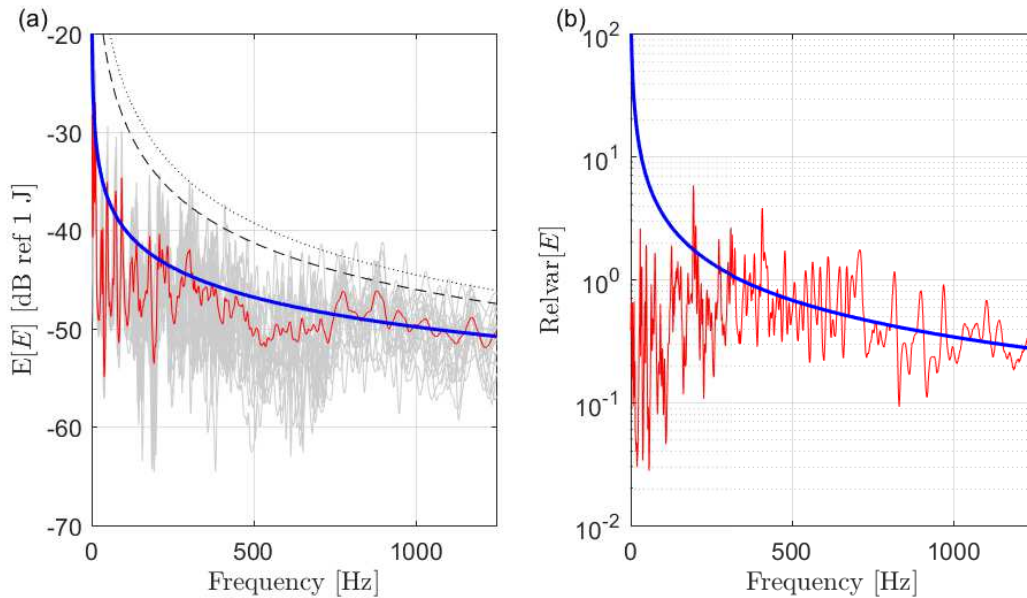
Figure 4: (a) Energy of the plate due to a unit point force excitation. Gray: response of the 20 members of the ensemble; red: experimental ensemble mean response; thick blue: hybrid method prediction; dashed black: 95% CI upper bound; dotted black: 99% CI upper bound. (b) Relative variance of the energy. Red: experimental ensemble variance; thick blue: hybrid method prediction.

In general, there is a good agreement between the measured plate ensemble average response and the response predicted by the hybrid model. The hybrid prediction seems to slightly overestimate the low-frequency response of the system and also the response in the range 450-700 Hz, a result that can be explained by the effect that the damping treatment has on the plate response. A good agreement has been also found in the relative variance results, with differences that are only significant at very low frequencies, where the ensemble of systems may not be random enough. The agreement in the average response could be slightly improved by using a frequency-dependent subsystem loss factor. However, as the differences observed

18

411 are acceptable, the authors have opted to use the frequency averaged constant loss factor previously defined

412 for the comparisons presented in Sections 4.1.3 and 4.1.4.

4.1.3. Coupled system. Results for an impact excitation

414 The response of the coupled electric pump-isolators-plate system to an impact excitation is considered

415 in this section. The excitation was applied, using an instrumented hammer, on the electric pump structure,

416 and the response was measured at three different locations of the receiver plate. As before, the responses

417 per unit force were computed dividing the measured acceleration spectra by the measured force spectrum.

418 The response of an ensemble of experimental subsystems was obtained by performing the test 20 times (with

419 different mass locations).

420 Figure 5(a) presents the response per unit force of the receiver plate to the impact excitations. The

421 responses of the three measuring accelerometers for all the 20 tests have been used to create an ensemble of

422 60 experimental realisations. The ensemble mean of the experimental modulus squared of the velocity has

423 been compared with the predicted response of the hybrid method. This prediction has been computed using

424 Equation (26) and the relation $\mathrm{E}[|v|^2] = 2\mathrm{E}[E]/m_\mathrm{p}$, where m_p has been considered to be the mass of the

425 receiver plate with the additional point masses. In this case, the set of blocked forces required by Equation

426 (23) and determined following the experimental procedure described in Section 2.2.2, are blocked forces per

427 unit of input force. Again, the upper CI for a 95% CL, and for a 99% CL have been computed assuming

428 that the statistical distribution of the plate energy is lognormal. In this case, the CLs are computed using

429 the relative variance of the energy density at a point (ε say), which is approximately related to the relative

430 variance of the total subsystem energy as follows [48]

$$\mathrm{Relvar}[|v|^2] = \mathrm{Relvar}[\varepsilon] = 1 + 2\mathrm{Relvar}[E]. \tag{30}$$

431 The relative variance predicted by the hybrid method, computed using Equations (26) and (27), has been

432 compared to the experimental relative variance of the response in Figure 5(b), and these values have been

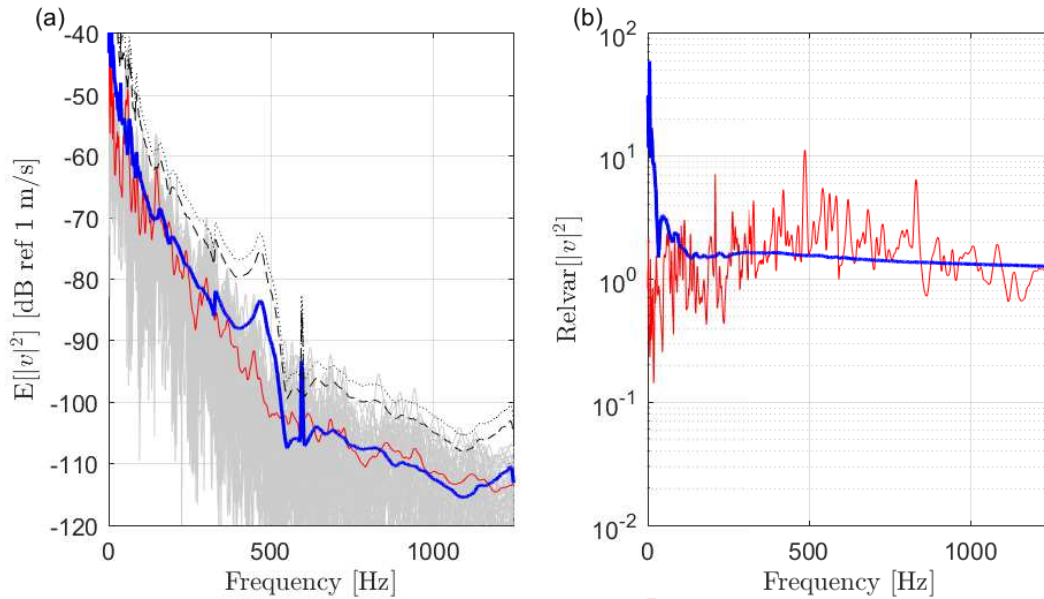433 used to produce the confidence intervals in Figure 5(a).

19

Figure 5: (a) Modulus squared of the velocity of the receiver plate due to a unit point force excitation in the first case study. Gray: response of the 60 members of the ensemble; red: experimental ensemble mean response; thick blue: hybrid method prediction; dashed black: 95% CI upper bound; dotted black: 99% CI upper bound. (b) Relative variance of the modulus squared of the velocity. Red: experimental ensemble variance; thick blue: hybrid method prediction.

In general, there is a good agreement between the measured plate ensemble average response and the response predicted by the hybrid model developed in this work. Significant discrepancies are only observed between 400 and 550 Hz and at 600 Hz, where the model predicts increases in the response that are not observed in the experimental results. These two peaks are mainly caused by an unexpectedly high amplitude of the characterised blocked forces and, as explained in the Appendix, these incorrect values are caused by consistency problems in the measurements. Solutions for overcoming this problem are currently being studied by the authors [47].

The relative variance of the experimental modulus squared velocity only differs significantly from the predicted result at very low frequencies. Moreover, it can be seen in Figure 5(a) that the predicted upper CIs satisfactorily enclose the ensemble of experimental results for those frequencies where the blocked force measurements do not show consistency problems. This agreement shows that the assumption of a lognormal distribution for the statistics of the subsystem response is reasonable. As mentioned previously, this is an expected result for the type of experiment performed [49].

4.1.4. Coupled system. Results for the operational excitation forces

This section considers the response of the receiver plate to the excitation generated by the electric pump operating. Again, the response of the plate subsystem was measured at three different locations and, in

order to build the ensemble of experimental subsystems, the test was performed for 20 randomisations of the point masses. The locations of the three accelerometers and the seven masses for each randomisation were the same as the ones used for the impact excitation.

Figure 6(a) presents the response of the receiver plate to the operational excitation forces. As before, an ensemble of 60 experimental realisations has been created combining the responses of the three accelerometers. An expanded view of a section of the Figure is shown in Figure 6(b). In this case, the blocked force contains a large number of strong harmonics, and these harmonics are propagated to the predicted response. Even in Figure 6(b), the comparison between the hybrid prediction and the experimental results is confused by the high degree of fluctuations in the curves.
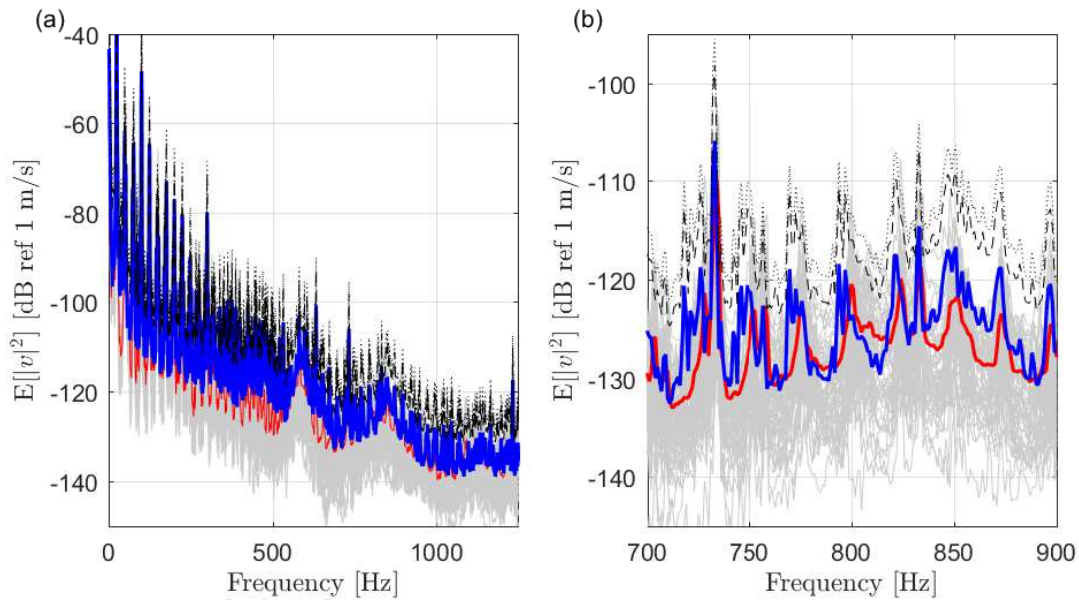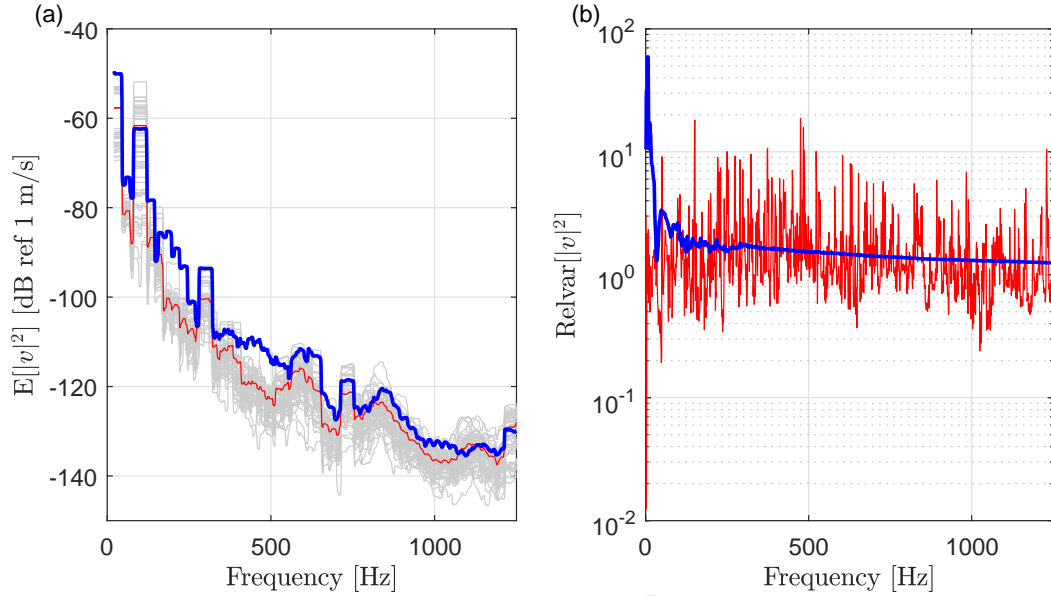

Figure 6: (a) Modulus squared of the velocity of the receiver plate for the running engine excitation (smoothed) in the first case study. Gray: response of the 20 members of the ensemble; red: experimental ensemble mean response; thick blue: hybrid method prediction; dashed black: 95% CI upper bound; dotted black: 99% CI upper bound. (b) Zoomed view of the results presented in(a).

An alternative comparison is presented in Figure 7 where, for clarity, the results have been smoothed by applying a running band average of width $\Delta f = 40$ Hz. As in the impact excitation case, there is a fairly good agreement between the experimental response of the plate and the response predicted by the hybrid model. In this case, significant differences are mainly observed between 150 and 250 Hz, and between 400 and 550 Hz. Again, the cause of these differences, which is discussed in more detail in the Appendix, is an overprediction of the characterised blocked forces. Figure 7(b) shows that a good agreement is also observed between the measured and the predicted relative variance of the response.

21

Figure 7: (a) Modulus squared of the velocity of the receiver plate for the running engine excitation (smoothed) in the first case study. Gray: response of the 20 members of the ensemble; red: experimental ensemble mean response; thick blue: hybrid method prediction. (b) Relative variance of the modulus squared of the velocity. Red: experimental ensemble variance; thick blue: hybrid method prediction.

4.2. Case study II: motor on a small plate/isolators/large thin plate

4.2.1. The test system and the experimental setup

The vibration source used in this case study, shown in Figure 2b, consisted of a servo motor bolted to a small aluminium plate, itself attached to four steel feet. Each foot was instrumented with two single axis accelerometers, spaced approx. 2.5cm apart. The source subsystem was again connected to a receiver large thin plate using four resilient elements. The construction of a hybrid model for this second assembly again required to characterise experimentally the source mobility, the blocked forces acting on the source-isolators interface and the dynamic stiffness of the isolators.

In the characterisation of its free mobility, the source was suspended on soft elastic bungees and each foot excited in four positions. Appropriate averaging of the spaced excitation and response measurements returned the free source mobility, $\mathbf{Y}_S \in \mathbb{C}^{4 \times 4}$.

In the characterisation of its blocked force the source was resiliently coupled to the intended installation and the coupled source mobility measured as per the above procedure. Note that the blocked force need not be characterised on the assembly in which predictions are made. This was done to avoid any variation in the excitation mechanism between the characterisation and validation phases.[1] The characterisation was

---

[1] In the first case study the source was characterised on a separate assembly, and the blocked forces were 'transferred' into the intended installation.

481 performed using only the coupling interface DoFs, i.e. $b = c$, thus no over-determination was performed.

482 Operational velocities were measured for both operational and artificially excited conditions. For repeata-

483 bility the operational velocities due to the artificial excitation were normalised to the input force. Having

484 averaged the spaced velocities appropriately, the blocked forces were found as per Section 2.2.2.

485 In this case each of the four resilient elements (type: Fibet 2525VV18-45) used in this study were

486 characterised using the in-situ approach presented in Section 2.3. Each element was used to construct a

487 mass-isolator-mass assembly, as illustrated in Figure 1b. A spaced pair of accelerometers were mounted

488 above and below the coupling element and excitations performed at each. The resulting mobilities were

489 averaged appropriately to yield the coupling interface mobility matrix, $\mathbf{Y}_C \in \mathbb{C}^{2 \times 2}$. The transfer stiffness

490 of each element was then determined as per Equations (19) and (20).

491 The receiver subsystem was the same aluminium plate considered in the first case study, but no damping

492 treatment was applied in this case. The loss factor of the plate was again experimentally determined from

493 its response without the deterministic subsystem, i.e. the source structure and the four isolators, placed on

494 it. The loss factor was found to be approximately constant in the frequency range of interest (1-1250 Hz),

495 with a value $\eta = 0.7\%$. With this value, the modal overlap factor at 1000 Hz is $m = \omega n \eta = 0.57$.

496 In order to create an ensemble of subsystems, the plate response was randomised experimentally by

497 adding 10 small masses at randomly chosen locations. The total mass added was 600 g, approximately 10%

498 of the initial mass of the plate.

499 Two types of excitations were studied with the source subsystem considered in this case study: an impact

500 excitation applied on the source structure using an instrumented hammer and the excitation caused by the

501 servomotor running at a constant speed of 2800 rpm. A summary of the results presented for this case study

502 can be seen in Table 1.

4.2.2. Results for an impact excitation

504 Figure 8(a) presents the response of the receiver plate for the case where an impact excitation was

505 applied on the source subsystem using an instrumented hammer. The impacts were applied on the small

506 plate structure and the responses per unit force were computed dividing the measured acceleration spectra

507 by the measured force spectrum. The plate response was measured at six different locations and the test

508 was performed for 20 randomisations of the point masses.

509 The responses of the six measuring accelerometers for all the 20 tests have been used to create an ensemble

510 of 120 experimental realisations. The ensemble mean of the experimental modulus squared of the velocity

511 has been compared with the predicted response of the hybrid method. As in the previous case study, the

512 upper CI for a 95% CL and for a 99% CL have been computed assuming that the statistical distribution

513 of the plate energy is lognormal. The relative variance predicted by the hybrid method, computed using

514 Equations (26) and (27), has been compared to the experimental relative variance of the response in Figure

23

515 8(b). Again, this relative variance has been used to produce the confidence intervals shown in Figure 8(a).
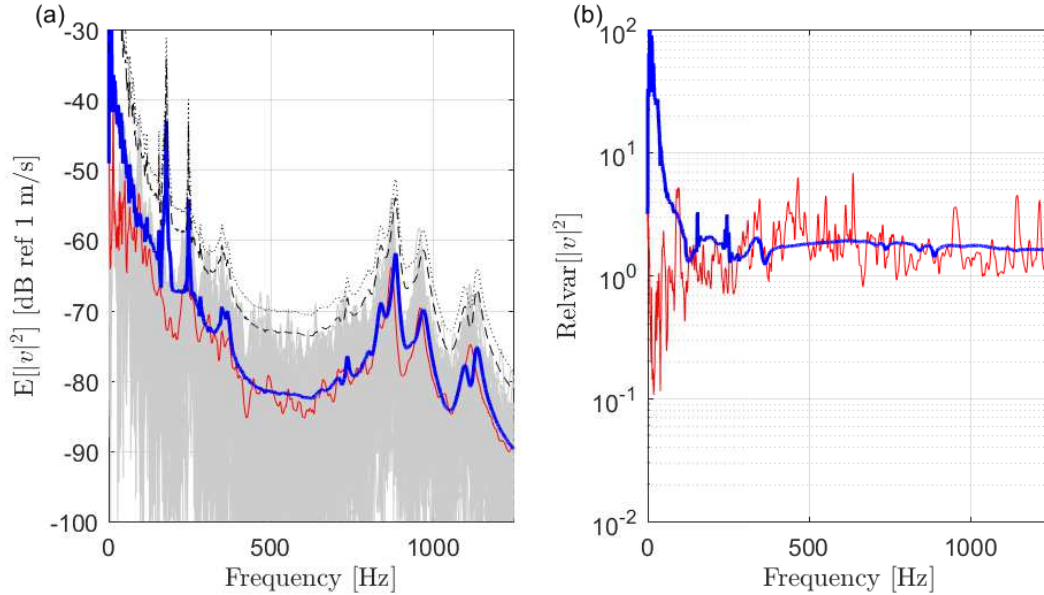

Figure 8: (a) Modulus squared of the velocity of the receiver plate due to a unit point force excitation in the second case study. Gray: response of the 120 members of the ensemble; red: experimental ensemble mean response; thick blue: hybrid method prediction; dashed black: 95% CI upper bound; dotted black: 99% CI upper bound. (b) Relative variance of the modulus squared of the velocity. Red: experimental ensemble variance; thick blue: hybrid method prediction.

516 The results show that there is a good agreement between the measured plate ensemble average response
517 and the response predicted by the hybrid model of this second case study. Significant discrepancies are
518 only observed at very low frequencies, and around 180 and 250 Hz, where the model predicts two sharp
519 peaks that are not observed in the experimental measures. Again, these peaks are caused by the consistency
520 problems that arise in the experimental determination of the blocked forces, as explained in the Appendix.

521 The good agreement between the experimental results and the predicted response can be also observed
522 in the relative variance results. The relative variance of the experimental modulus squared velocity only
523 differs significantly from the predicted result at very low frequencies. Moreover, it can be seen in Figure 8(a)
524 that the predicted upper CIs are satisfactorily enclosing the ensemble of experimental results, showing once
525 more that the experimental results support the assumption of a lognormal distribution for the statistics of
526 the subsystem response [49].

527 An ensemble of 20 experimental estimations of the plate energy has been obtained from the experimental
528 results using that $E = m_{\mathrm{p}} \langle |v|^2 \rangle_{\mathrm{a}}/2$. A comparison between the mean and relative variance of the experi-
529 mental energy, and the responses predicted by the hybrid model, computed again using Equations (26) and
530 (27), is shown in Figure 9. As before, the upper CI for a 95% and a 99 % CLs have been included in the
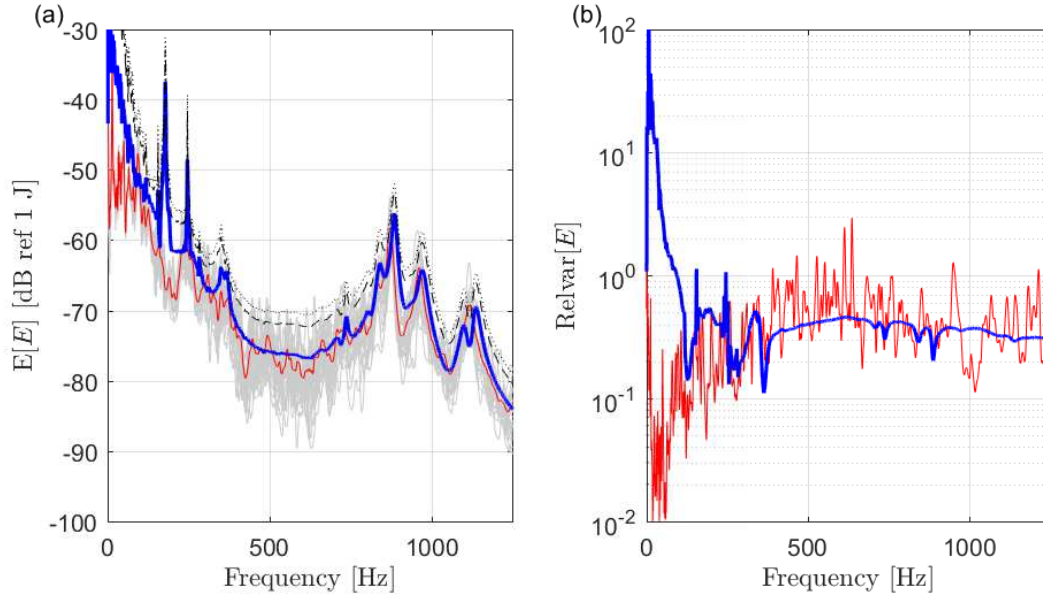
24

energy comparison.

Figure 9: (a) Energy of the receiver plate due to a unit point force excitation in the first case study. Gray: response of the 20 members of the ensemble; red: experimental ensemble mean response; thick blue: hybrid method prediction; dashed black: 95% CI upper bound; dotted black: 99% CI upper bound. (b) Relative variance of the energy. Red: experimental ensemble variance; thick blue: hybrid method prediction.

Again, there is a good agreement between the mean and variance of the energy predicted by the hybrid method and the experimental results. The main discrepancies observed are again the significant differences at low frequencies and the two peaks at 180 and 250 Hz. The space average performed in the experimental results has reduced significantly the variability of the ensemble responses and this effect has been properly caught by the hybrid model, which predicts a lower relative variance and, due to this, lower upper CIs. It should be mentioned that the experimental energy has been estimated by performing a space average of the response at only six positions and it is reasonable to expect that taking measurements at a larger number of positions would reduce the fluctuations in the experimental relative variance.

4.3. Results for a running motor

Figure 10(a) presents the response of the receiver plate for the case where the servomotor of the source subsystem was running at a constant speed of 2800 rpm. As in the previous excitation case, the response of the plate subsystem was measured at six different locations and the test was performed for 20 randomisations of the point masses. The locations of the six accelerometers and the 10 masses for each randomisation were the same as the ones used for the impact excitation. For clarity, the results have been smoothed by applying a frequency running average with a bandwidth $\Delta f = 40$ Hz.
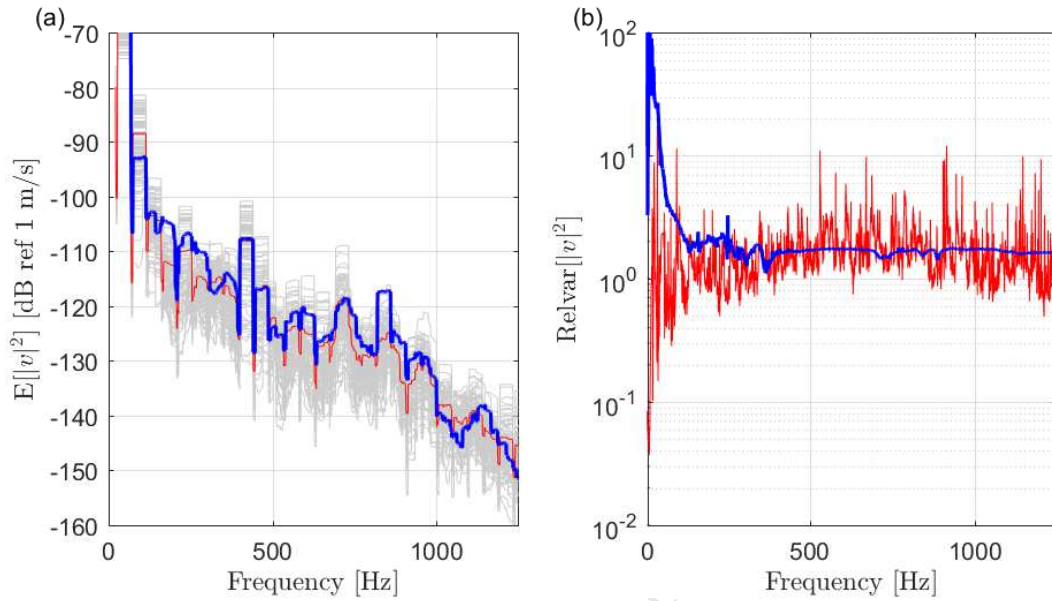
25

Figure 10: (a) Modulus squared of the velocity of the receiver plate for the running engine excitation (smoothed). Gray: response of the 120 members of the ensemble; red: experimental ensemble mean response; thick blue: hybrid method prediction. (b) Relative variance of the modulus squared of the velocity. Red: experimental ensemble variance; thick blue: hybrid method prediction.

As in the impact excitation case, there is a good agreement between the experimental response of the plate and the response predicted by the hybrid model. A good agreement is also observed for the relative variance, as shown in Figure 10(b).

The mean and relative variance of the vibrational energy of the plate predicted by the hybrid method are compared with their corresponding experimental values in Figure 11. The results again show that the predicted mean response agrees very well with the experimental results, but the hybrid model slightly underpredicts the relative variance of the structure. As in the impact excitation case, it is reasonable to assume that the differences observed would be reduced if a larger number of accelerometers were used to estimate the plate energy.
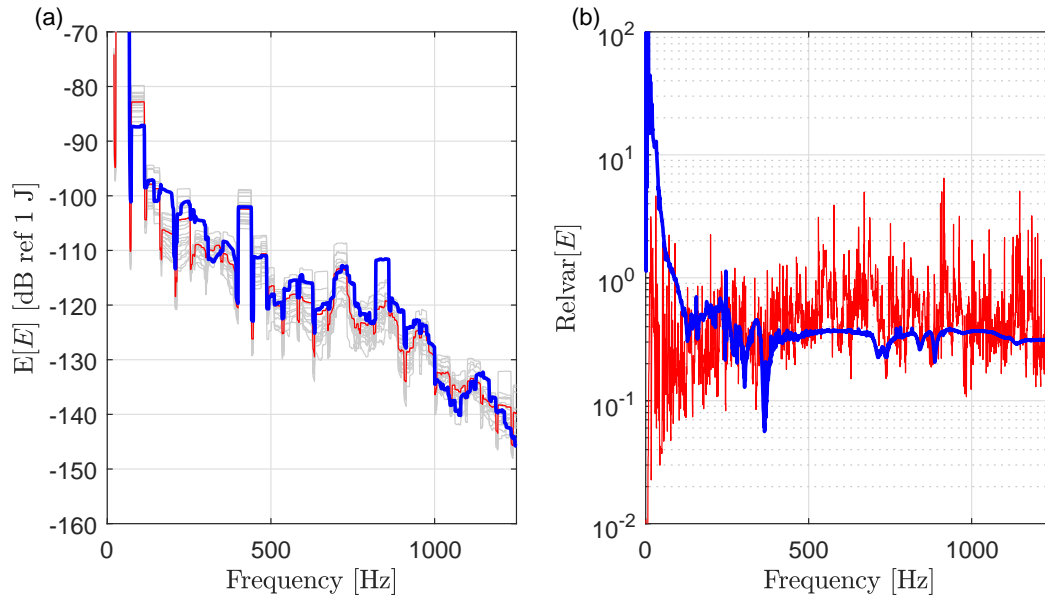
Figure 11: (a) Energy of the receiver plate for the running engine excitation (smoothed). Gray: response of the 20 members of the ensemble; red: experimental ensemble mean response; thick blue: hybrid method prediction. (b) Relative variance of the energy. Red: experimental ensemble variance; thick blue: hybrid method prediction.

5. Conclusion

This paper has presented a hybrid FE-SEA-experimental methodology for predicting the mid-frequency response of random dynamic systems. The proposed methodology combines the use of experimentally characterised structures with a previously developed hybrid FE-SEA numerical formulation [8, 12]. The methodology has been successfully applied to two case studies consisting of a vibration source coupled with isolators to a large thin receiver plate. These case studies show that both active (e.g., motors) and passive (e.g., vibration isolators) experimentally determined subsystems can be included in the new formulation.

The proposed approach yields predictions for the ensemble mean and variance of the response of a random system, and confidence bands on this response can also be established. The method implicitly assumes that GOE statistics can be used to model the uncertainty in the SEA subsystems (in the case studies, a random plate) and this avoids the need for detailed information regarding the nature of the uncertainty, and also the need for Monte Carlo simulations. The approach has been shown to yield to good agreement with benchmark experimental results for randomised systems. One issue that has been found with the experimental characterisation of the vibration sources is that the use of the measured blocked forces can on rare occasions lead to unexpected sharp peaks in the predicted response. It has been shown that these peaks can be explained by the sensitivity of the determined blocked forces to experimental errors. Care is needed to try to identify these false peaks in the modelling process. This issue is left as further work.

27

573 It can be concluded that the approach can be used to extend the existing FE-SEA method [8, 12] to
574 systems which contain components that cannot be modelled analytically, and therefore require experimental
575 characterisation. The result is an efficient methodology which reduce modelling effort by employing SEA
576 and experimental results, and which yields a detailed statistical description of the response.

Acknowledgements

Appendix A. Sensitivity of the blocked force determination

581 The sensitivity of the determined blocked force to experimental errors is studied in this appendix using
582 a simple hybrid FE-SEA model. The considered system, shown in Figure A.1, consists of three point
583 masses (m_1, m_2 and m_3) connected in series with two spring elements (with stiffness constants k_1 and k_2,
584 respectively). The lower mass, m_3, is considered to be perfectly attached to a large thin plate and the whole
585 system is excited by a vertical unitary harmonic point load, $f_{\text{ext}} = 1$, applied on the upper mass m_1.

586 The deterministic part of the system is assumed to consist of three-DoF (q_1-q_3) representing the vertical
587 response of the three point masses. The response of q_2, q_3 and of the receiver plate (defined by its vibrational
588 energy E) to the external excitation is equivalent to that obtained by considering the following blocked force
589 applied at q_2

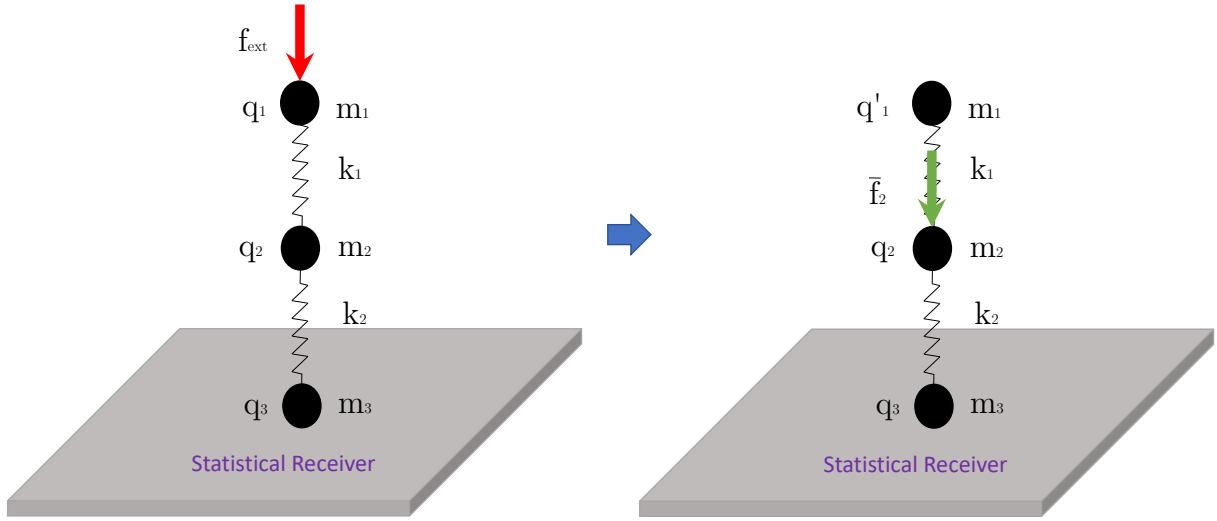$$\bar{f}_2 = \frac{1}{1 - m_1\omega^2/k_1}. \tag{A.1}$$

Figure A.1: Analytical 3DoF-plate model with the external excitation considered (left) and its corresponding blocked force excitation at q_2 (right).

The matrices required to compute the hybrid mean and variance equations for the analytical model are

$$\mathbf{D}_{\mathrm{d}} = \begin{bmatrix} k_1 - m_1\omega^2 & -k_1 & 0 \\ -k_1 & k_1 + k_2 - m_2\omega^2 & -k_2 \\ 0 & -k_2 & k_2 - m_3\omega^2 \end{bmatrix}, \tag{A.2}$$

$$\mathbf{D}_{\mathrm{dir}} = \begin{bmatrix} 0 & 0 & 0 \\ 0 & 0 & 0 \\ 0 & 0 & 8\mathrm{i}\omega\sqrt{D\rho h} \end{bmatrix}, \tag{A.3}$$

$$\mathbf{S}_{ff} = \begin{bmatrix} 0 & 0 & 0 \\ 0 & \bar{f}_2\bar{f}_2^* & 0 \\ 0 & 0 & 0 \end{bmatrix}, \tag{A.4}$$

where it has been assumed that the applied excitation is the blocked force defined by Equation (A.1).

The blocked force can also be expressed in terms of the free mobilities of the subsystem $m_1 - k_1 - m_2$ as follows

$$\bar{f}_2 = Y_{22}^{-1} v_{2,fs} = Y_{22}^{-1} Y_{21}, \tag{A.5}$$

where $v_{2,fs}$ is the free velocity of q_2 and where

$$Y_{22} = (k_1 - m_1\omega^2)\Delta, \qquad Y_{21} = k_1\Delta, \tag{A.6}$$

29

597 with $\Delta = \dfrac{\mathrm{i}\omega}{(k_1 - m_1\omega^2)(k_1 - m_2\omega^2) - k_1^2}$.

598

599   The effect of adding an artificial numerical error to the measured mobilities can be assessed by considering

600 measured mobilities $Y_{21}^{\mathrm{m}} = Y_{21} + \epsilon_1$ and $Y_{22}^{\mathrm{m}} = Y_{22} + \epsilon_2$, where ϵ_i are small errors added to the measurement.

601 The effect that adding this small artificial errors has on the response of the system is shown in Figure A.2.

602 The results have been computed considering $m_1 = 2$ kg, $m_2 = 2.5$ kg, $m_3 = 0.25$ kg, $k_1 = 10^6$ N/m, $k_2 =$

603 10^5 N/m. Structural damping has been added considering a complex valued stiffness $k_i^c = k_i(1 + \mathrm{i}\eta)$, with

604 $\eta = 0.01$. For each computed frequency, the error quantities ϵ_i have been considered to have a constant

605 amplitude and a random phase. These amplitudes have been considered to be equal to 0.2% of the maximum

606 amplitude of the mobilities in the range of frequencies studied (50-200 Hz).

607   The results highlight how sensitive is the blocked force determination to measuring errors at antireso-

608 nances of Y_{22}. As can be seen in Figures A.2(c) and (d), this error may cause an incorrect characterisation

609 of the blocked force, which results in an incorrect prediction of the receiver plate energy. A general descrip-

610 tion of this experimental inconsistency, not limited to the type of hybrid models presented in this work,

611 can be found in [47]. It is worth noting that similar errors are often encountered in experimental dynamic

612 sub-structuring, although in this case they stem from inconsistencies in measured FRF matrices [39], as
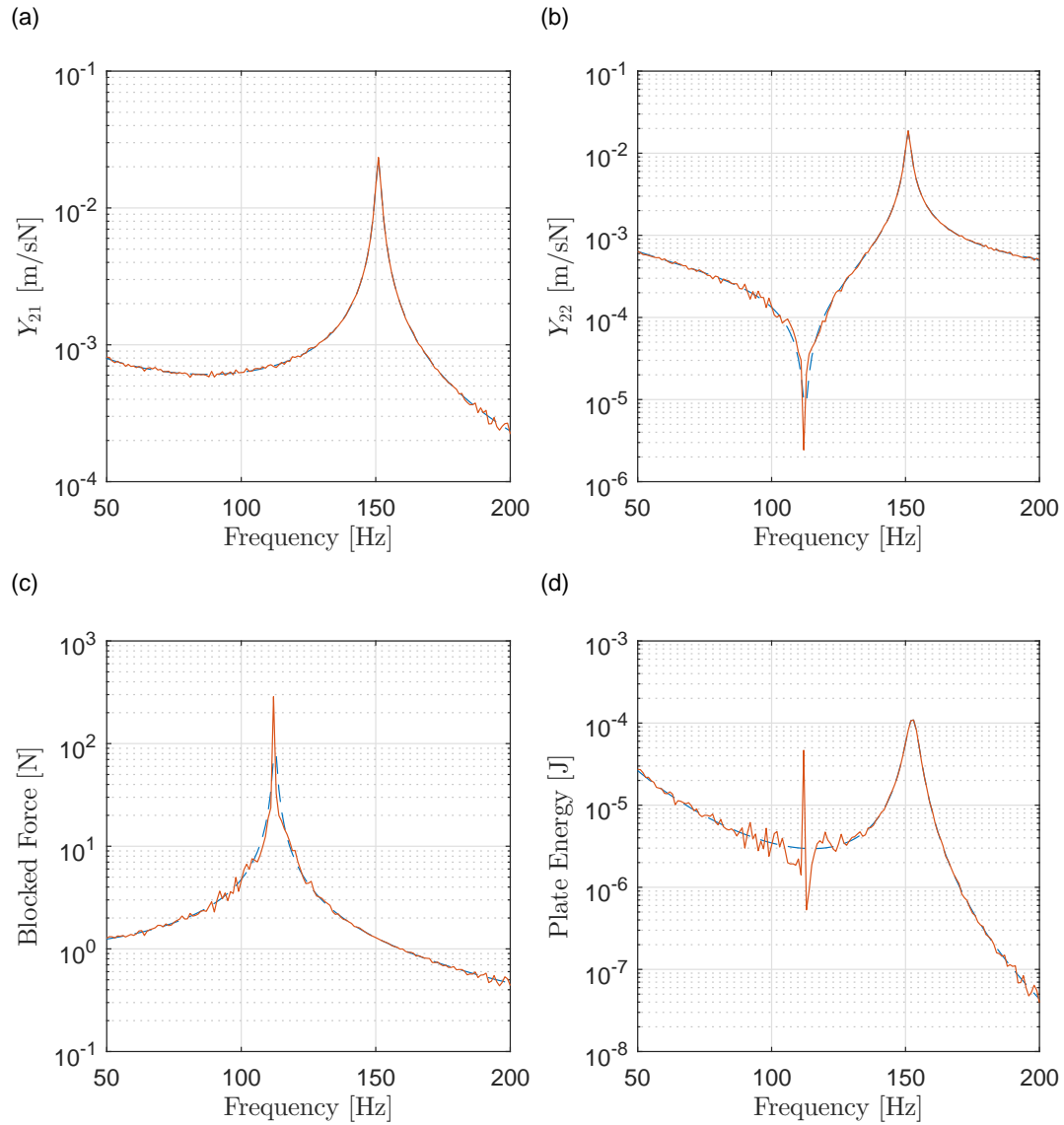
613 opposed to blocked forces.

30

Figure A.2: Results for the simple 3 DoF-plate model with (solid line) and without (dashed line) a numerical error. (a) Mobility Y_{21}. (b) Mobility Y_{22}. (c) Magnitude of the blocked force applied on q_2. (d) Energy of the receiver plate.

References

615 [1] P. Rouch, P. Ladeveze, The variational theory of complex rays: a predictive tool for medium-frequency vibrations, Com-
616   puter Methods in Applied Mechanics and Engineering 192 (28-30) (2003) 3301–3315.

617 [2] W. Desmet, A wave based prediction technique for coupled vibro-acoustic analysis, Ph.D. thesis (1998).

618 [3] R. Tezaur, C. Farhat, Three-dimensional discontinuous galerkin elements with plane waves and lagrange multipliers for

the solution of mid-frequency helmholtz problems, International Journal for Numerical Methods in Engineering 66 (5) (2006) 796–815.

[4] R. Lyon, R. DeJong, Theory and Application of Statistical Energy Analysis, Butterworth-Heinemann, Boston, 1995.

[5] R. S. Langley, V. Cotoni, Response variance prediction in the statistical energy analysis of built-up systems, The Journal of the Acoustical Society of America 115 (2) (2004) 706.

[6] L. Maxit, J.-L. Guyader, Calculation of sea coupling loss factors using the dual formulation and fem modal information part i: Theory, Journal of sound and vibration (2001) 907–930.

[7] R. J. Bernhard, J. E. Huff, Structural-acoustic design at high frequency using the energy finite element method, Journal of Vibration and Acoustics 121 (3) (1999) 295–301.

[8] P. Shorter, R. Langley, Vibro-acoustic analysis of complex systems, Journal of Sound and Vibration 288 (3) (2005) 669–699.

[9] P. Shorter, R. Langley, On the reciprocity relationship between direct field radiation and diffuse reverberant loading, The Journal of the Acoustical Society of America 117 (1) (2005) 85–95.

[10] R. Langley, On the diffuse field reciprocity relationship and vibrational energy variance in a random subsystem at high frequencies, Journal Acoustical Society of America 121 (2) (2007) 913–921.

[11] V. Cotoni, P. Shorter, R. Langley, Numerical and experimental validation of a hybrid finite element-statistical energy analysis method, The Journal of the Acoustical Society of America 122 (1) (2007) 259–270.

[12] R. Langley, V. Cotoni, Response variance prediction for uncertain vibro-acoustic systems using a hybrid deterministic-statistical method., The Journal of the Acoustical Society of America 122 (6) (2007) 3445–63.

[13] A. Cicirello, R. Langley, The vibro-acoustic analysis of built-up systems using a hybrid method with parametric and non-parametric uncertainties, Journal of Sound and Vibration 332 (9) (2013) 2165–2178.

[14] A. Cicirello, R. S. Langley, Efficient parametric uncertainty analysis within the hybrid Finite Element/Statistical Energy Analysis method, Journal of Sound and Vibration 333 (6) (2014) 1698–1717.

[15] B. Cimerman, T. Bharj, G. Borello, Overview of the experimental approach to statistical energy analysis, in: Proceedings of the SAE Noise and Vibration Conference, paper 97NV169, 1997.

[16] D. A. Bies, S. Hamid, In situ determination of loss and coupling loss factors by the power injection method, Journal of Sound and Vibration 70 (2) (1980) 187–204.

[17] N. Lalor, Practical considerations for the measurement of internal and coupling loss factors on complex structures, Technical report, ISVR (1990).

[18] M. Rosen, G. Borello, Damping and coupling loss factors estimation in sea method; what is really measured?, in: International congress on noise control engineering, 1996, pp. 2903–2908.

[19] C. Hopkins, Experimental statistical energy analysis of coupled plates with wave conversion at the junction, Journal of Sound and Vibration 322 (1-2) (2009) 155–166.

[20] O. Guasch, A direct transmissibility formulation for experimental statistical energy analysis with no input power measurements, Journal of Sound and Vibration 330 (25) (2011) 6223–6236.

[21] F. Fahy, J. Walker (Eds.), Advance Applications in Acoustics, Noise and Vibration, Spoon Press, 2004.

[22] A. Moorhouse, A. Elliott, T. Evans, In situ measurement of the blocked force of structure-borne sound sources, Journal of Sound and Vibration 325 (4-5) (2009) 679–685.

[23] D. Klerk, Dynamic response characterization of complex systems through operational identification and dynamic substructuring, Ph.D. thesis, TU Delft (2009).

[24] D. De Klerk, D. J. Rixen, Component transfer path analysis method with compensation for test bench dynamics, Mechanical Systems and Signal Processing 24 (6) (2010) 1693–1710.

[25] A. S. Elliott, A. T. Moorhouse, T. Huntley, S. Tate, In-situ source path contribution analysis of structure borne road noise, Journal of Sound and Vibration 332 (24) (2013) 6276–6295.

[26] D. Lennström, M. Olsson, F. Wullens, A. Nykänen, Validation of the blocked force method for various boundary conditions for automotive source characterization, Applied Acoustics 102 (2016) 108–119.

[27] T. Alber, M. Sturm, A. Moorhouse, Independent characterization of structure-borne sound sources using the in-situ blocked force method, in: Proceedings of Internoise, 2016, pp. 7302–7313.

[28] M. Sturm, T. Alber, A. Moorhouse, D. Zabel, Z. Wang, The in-situ blocked force method for characterization of complex automotive structure-borne sound sources and its use for virtual acoustic prototyping, in: Proceedings of ISMA2016 including USD2016, 2016.

[29] M. W. F. Wernsen, M. V. v. d. Seijs, D. d. Klerk, An indicator sensor criterion for in-situ characterisation of source vibrations, in: Sensors and Instrumentation, Volume 5. Conference Proceedings of the Society for Experimental Mechanics Series, 2017, pp. 55–69.

[30] D. Zabel, M. Sturm, T. Alber, A. Moorhouse, Embedded MEMS accelerometers for the in-situ measurement of blocked forces in coupled structures, in: DAGA 2017 Kiel, 2017, pp. 423–426.

[31] M. Sturm, M. Yankonis, R. Bosch, C. Marchand, S. Sherman, J. Hirscher, M. Priebe, P. Parikh, A. Moorhouse, Robust NVH Development of Steering Systems Using In-Situ Blocked Forces from Measurements with Low-Noise Driver Simulators, in: Noise-Con, Grand Rapids, MI, 2017.

[32] H. Lai, Alternative test methods for measuring structure-borne sound power, in: Internoise, Honolulu, Hawaii, USA, 2006.

[33] G. Banwell, R. Faventi, Assessment of experimental techniques to characterise the vibration source strength of a motor radially mounted with resilient elements, in: Proceedings of ISMA2016 including USD2016, 2016.

[34] A. Elliott, A. Moorhouse, In-situ characterisation of structure borne noise from a building mounted wind turbine, Proceedings of ISMA2010 (2010) 2055–2068.

[35] R. Langley, A. Brown, The ensemble statistics of the energy of a random system subjected to harmonic excitation, Journal of Sound and Vibration 275 (3-5) (2004) 823–846.

[36] R. S. Langley, V. Cotoni, The ensemble statistics of the vibrational energy density of a random system subjected to single point harmonic excitation, Journal Acoustical Society of America 118 (5) (2005) 3064–3078.

[37] S. Voormeeren, D. Rixen, A family of substructure decoupling techniques based on a dual assembly approach, Mechanical Systems and Signal Processing 27 (2012) 379–396.

[38] J. Meggitt, A. Moorhouse, In-situ sub-structure decoupling of resiliently coupled assemblies, Mechanical Systems and Signal Processing 117 (2019) 723 – 737.

[39] D. Rixen, How measurement inaccuracies induce spurious peaks in frequency based substructuring, in: IMAC XVI, Orlando, FL, 2008.

[40] R. Penrose, J. Todd, A generalized inverse for matrices, Mathematical Proceedings of the Cambridge Philosophical Society 51 (03) (1955) 406.

[41] J. Verheij, Multi-path sound transfer from resiliently mounted shipboard machinery, Ph.D. thesis (1982).

[42] International Organization for Standardization, BS EN ISO 10846-1:2008 Acoustics and vibration - Laboratory measurement of vibroacoustic transfer properties of resilient elements, Part 1: Principles and guidelines (2008).

[43] J. Meggitt, A. Elliott, A. Moorhouse, In-situ determination of dynamic stiffness for resilient elements, Proc IMechE Part C: J Mechanical Engineering Science 230 (6) (2016) 986–993.

[44] J. Meggitt, On In-situ Methodologies for the Characterisation and Simulation of Vibro-Acoustic Assemblies, Phd, University of Salford (2017).

[45] L. Cremer, M. Heckl, E. Ungar, Structure-borne sound, Springer-Verlag, Berlin, 1985.

[46] J. Meggitt, A. Elliott, A. Moorhouse, Virtual assemblies and their use in the prediction of vibro-acoustic responses, in: Proceedings of the Institute of Acoustics, Warickshire, 2016.

[47] J. Meggitt, A. Moorhouse, A. Elliott, A. Clot, R. Langley, Development of a hybrid FE-SEA-experimental model: exper-

705   imental sub-system characterisation, in: Proceedings of NOVEM 2018, 2018.

706   [48] V. Cotoni, R. Langley, M. Kidner, Numerical and experimental validation of variance prediction in the statistical energy

707   analysis of built-up systems, Journal of Sound and Vibration 288 (3) (2005) 701–728.

708   [49] R. Langley, J. Legault, J. Woodhouse, E. Reynders, On the applicability of the lognormal distribution in random dynamical

709   systems, Journal of Sound and Vibration 332 (13) (2013) 3289–3302.